

Tailored Thioxanthone-Based Photoinitiators for Two-Photon-Controllable Polymerization and Nanolithographic Printing

Teng Chi,¹ Paul Somers,² Daniel A. Wilcox,³ Ashley J. Schuman,¹ Vasudevan Iyer,² Ran Le,² Jamie Gengler,^{4,5} Manuel Ferdinandus,^{4,6} Carl Liebig,⁴ Liang Pan,² Xianfan Xu,² Bryan W. Boudouris ^{1,3}

¹Department of Chemistry, Purdue University, 560 Oval Drive, West Lafayette, Indiana, 47907

²School of Mechanical Engineering and Birck Nanotechnology Center, Purdue University, West Lafayette, Indiana, 47907

³Charles D. Davidson School of Chemical Engineering, Purdue University, 480 W Stadium Ave, West Lafayette, Indiana, 47907

⁴Air Force Research Laboratory, 2179 12th St., Wright-Patterson Air Force Base, Ohio, 45433

⁵UES Inc., 4401 Dayton-Xenia Rd, Dayton, Ohio, 45432

⁶Air Force Institute of Technology, 2950 Hobson Way, Wright Patterson AFB, Ohio, 45433

Correspondence to: B. W. Boudouris (E-mail: boudouris@purdue.edu)

Received 14 May 2019; revised 15 September 2019; accepted 1 October 2019

DOI: 10.1002/polb.24891

ABSTRACT: Printing of high-resolution three-dimensional nanostructures utilizing two-photon polymerization has gained significant attention recently. In particular, isopropyl thioxanthone (ITX) has been implemented as a photoinitiator due to its capability of initiating and depleting polymerization on demand, but new photoinitiating materials are still needed in order to reduce the power requirements for the high-throughput creation of 3D structures. To address this point, a suite of new thioxanthone-based photoinitiators were synthesized and characterized. Then two-photon polymerization was performed using the most promising photoinitiating molecule. Importantly, one of the initiators, 2,7-bis[4-(dimethylamino)phenyl ethynyl]-9H-thioxanthen-9-one] (BDAPT), showed a fivefold improvement in the writing threshold over the commonly used ITX

molecule. To elucidate the fundamental mechanism, the excitation and inhibition behavior of the BDAPT molecule were evaluated using density functional theory (DFT) calculations, low-temperature phosphorescence spectroscopy, ultra-fast transient absorption spectroscopy, and the two-photon Z-scan spectroscopic technique. The improved polymerization threshold of this new photoinitiator presents a clear pathway for the modification of photoinitiators in 3D nanoprinting. © 2019 Wiley Periodicals, Inc. *J. Polym. Sci., Part B: Polym. Phys.* 2019

KEYWORDS: 3D nanoprinting polymerizations; direct laser writing; thioxanthone-based photoinitiators; two-photon polymerization; ultrafast transient absorption spectroscopy

INTRODUCTION Two-photon polymerization was first reported in 1997,¹ and this has caused rapid growth in the field of nanolithography. A type of direct laser writing (DLW), this two-photon polymerization printing process takes advantage of the nonlinearity of multiphoton absorption in a polymeric photoresist to improve the spatial confinement of the printed voxel in a significant manner. In turn, this allows for the polymerization to occur inside the monomeric photoresist, and the fabrication of arbitrary 3D structures with submicron resolution is achieved.^{1,2} DLW has been highlighted in recent years as a high-speed and low-cost tool for generating high-fidelity 3D nanoscale features in fields such as photonics^{3,4} and tissue engineering.^{5,6} While the spatial resolution of DLW is significantly improved relative to analogous single-photon

polymerization systems, it remains a diffraction-limited process. This significant barrier can be overcome by introducing a polymerization-inhibiting depletion laser.⁷ That is, in a concept first applied to microscopy,⁸ the resolution of DLW was improved by spatially overlapping a shaped depletion laser beam such that the DLW beam is positioned in a minimum of the depletion laser beam.⁹ In this configuration, the photo-initiated polymerization is inhibited anywhere outside of the depletion laser minimum. Critical to the success of this inhibition-based polymerization technique is the optical response of the photoinitiating species in the DLW process. That is, the photoinitiator must allow for efficient initiation (and subsequent propagation) of the polymerization by the excitation beam while the inhibition beam must stop the polymerization reaction in an effective manner. To this end,

Additional Supporting Information may be found in the online version of this article.

†Teng Chi and Paul Somers contributed equally to this work.

© 2019 Wiley Periodicals, Inc.

several two-photon photoinitiating species have been developed, and some of the most promising materials have been investigated with nanolithographic applications in mind.^{10,11} However, there is a demand in both academic and industrial circles for more efficient photoinitiators in order to reduce the writing laser power requirements. Because the polymerization that the photoinitiator controls is key in the DLW process, we synthesized a series of new thioxanthone-based photoinitiators in order to achieve more efficient initiation (i.e., lower power) of the photopolymerizations at the nanoscale, and we established that the appropriate design of these materials and the modulation of their photophysical properties can significantly reduce the power required to create two-photon polymerized nanostructures.

The proposed photoinitiator builds from the fact that isopropyl thioxanthone (ITX) is an established photoinitiator in two-photon nanolithographic processes.¹² Despite the fact that ITX demonstrates the desired photoinitiation and photoinhibition properties with respect to the writing and depletion wavelengths,^{9,12} the writing laser power required for this material is still large at the common writing wavelength of 800 nm due to the weak two-photon absorption cross section of the ITX molecule.¹³ While not a particular issue for previously reported proof-of-concept demonstrations, reducing the amount of power required for photoinitiation is of critical import for scalable nanomanufacturing (i.e., in cases where multiple lasers would be required in order to achieve high-throughput production). Also of concern is the tendency of larger laser powers to lead to parasitic polymerization due to thermal initiation events, which can impact the minimum feature sizes that are attainable.¹⁴ Thus, there is a significant need to develop next-generation ITX derivatives that are capable of having improved light absorption profiles for the DLW wavelength ($\lambda = 800$ nm).

From nonlinear optics, the two-photon absorption coefficient is predicted to be optimal for an incident photon energy that is 0.7 times the bandgap of a wide bandgap material.¹⁵ In terms of designing a molecule for a constant DLW wavelength of 800 nm, this indicates a necessity to redshift the absorption peak of the photoinitiators relative to ITX to improve this ratio of absorption peak wavelength to the incident light wavelength. Moreover, it has been shown that molecules following a donor–acceptor–donor type structure also demonstrate an improved two-photon absorption cross section.¹⁶ Following these lines of thinking, we strive to take ITX and develop derivatives with improved two-photon absorption (i.e., increasing the number of initial electrons that are promoted to the singlet state) while studying the resulting effects on the polymerization initiating and inhibiting properties of the new compounds (i.e., we will evaluate the intersystem crossing processes and triplet state dynamics as well). We propose that the introduction of chromophores or electron donors leads to the generation of the donor–acceptor–donor or donor–acceptor species, and this will cause a redshift in the absorption spectrum. Compared to ITX, these derivatives should demonstrate improved two-photon absorption cross

sections. In order to accomplish this objective, the functional groups pendant to the thioxanthone-9-one core of ITX were tuned in a systematic manner. Specifically, phenyl, diphenyl, and naphthyl groups were attached to the ITX core with alkyne bridges, which leads to extended aromatic systems along the small molecule backbone. This extended conjugation, in turn, results in a bathochromic shift in the peak of the absorbance spectra of the molecules. Dialkylamino groups were added to terminate the ends of the molecules due to the strong electron-donating features of these substituents. In addition, mono- and di-substituted derivatives were synthesized and compared in order to elucidate the influence of the numbers of pendant groups on the photophysical properties of the polymerization initiators. The absorption spectra of the new initiators were predicted by density functional theory (DFT) calculations in order to provide a guide for the synthesis. Two-photon absorption cross sections were measured for each of the synthesized photoinitiators to provide a direct indicator of the DLW polymerization performance. The existence of possible charge transfer states that could arise due to the donor–acceptor molecular motif were rationalized by calculating the frontier molecular orbitals of the molecules. Ultra-fast transient absorption spectroscopy and phosphorescence spectra were utilized to determine excited state lifetimes in order to benchmark the polymerization inhibition characteristics and possible mechanism of the newly synthesized polymerization photoinitiators in comparison to ITX. DLW polymerization was then performed using the most-promising photoinitiator based on these evaluations, and the photoinitiating molecule, 2,7-bis[[4-(dimethylamino)phenyl ethynyl]-9H-thioxanthone-9-one] (BDAPT), demonstrated a reduction in required laser power for DLW when pentaerythritol triacrylate (PETA) served as the monomer for the polymerizations associated with the engineered photoinitiators. The writing laser power of BDAPT was reduced by fivefold relative to the laser power required for the same monomer system using the commonly implemented ITX photoinitiator. Therefore, the archetype presented here is one that sets a path forward in designing next-generation photoinitiators for their application towards low-power, high-throughput photopolymerizations in 3D nanoprinted materials.

EXPERIMENTAL

General Experimental Procedures

All chemicals were purchased from Sigma-Aldrich, and the chemicals were used as received. The ¹H NMR spectra were measured on a Bruker DRX500 spectrometer using a ~1% polymer solution (by weight) in deuterated chloroform (Sigma-Aldrich). Ultraviolet–visible (UV–Vis) spectroscopy data were collected using a Cary 60 spectrometer in the wavelength range of 330 nm $\leq \lambda \leq$ 800 nm. Fluorescence and phosphorescence spectroscopy data were obtained using a Cary Eclipse fluorescence and phosphorescence spectrophotometer in the wavelength range of 400 nm $\leq \lambda \leq$ 800 nm (with an excitation wavelength of 350 nm). Phosphorescence data were collected using deoxygenated solutions of the samples in a glass-forming solvent, with an absorbance below 0.01 at the excitation

wavelength. 9,10-Diphenylanthracene was used as a fluorescence quantum yield standard (94%) as the quantum yield of this material in THF is well established.¹⁷ In order to correct for solvent effects, eq 1 was utilized to normalize the quantum yield obtained for the 9,10-diphenylanthracene when PETA was the solvent.¹⁸

$$\Phi_{\text{PETA}} = \Phi_{\text{THF}} \left(\frac{S_{\text{PETA}}}{S_{\text{THF}}} \right) \left(\frac{n_{\text{PETA}}^2}{n_{\text{THF}}^2} \right) \quad (1)$$

Here, Φ_{THF} (94%) is the fluorescence quantum yield of the standard in THF. S_{THF} ($\sim 2.64 \times 10^6$ counts/a.u.) represents the slope of the integrated fluorescence signal obtained for the standard molecule vs. absorbance for different concentrations when they are dissolved in THF, and S_{PETA} ($\sim 2.50 \times 10^6$ counts/a.u.) represents the same slope when the standard molecule is dissolved in PETA. The refractive indices ($n_{\text{PETA}} = 1.483$ and $n_{\text{THF}} = 1.407$) were obtained from Sigma-Aldrich. From this equation, the fluorescence quantum yield of 9,10-diphenylanthracene in PETA was calculated as 98.7%. The quantum yield values of different photoinitiators were tested and referenced to the value of 9,10-diphenylanthracene.

Synthesis of Dibromo-9H-Thioxanthene-9-One (DBTX)

Thioxanthene-9-one (Compound 7, 4 g, 19.2 mmol) was added to a 500 mL round bottle flask with 32 mL of acetic acid. Then, 8 mL of bromine were added in a dropwise manner while the reaction mixture was held at 0 °C. After the addition of the bromine, the flask was slowly heated to 118 °C. After 24 h, a dark red solution formed, and at this time, the solution was poured into an ice bath. A yellow precipitate appeared, and it was filtered. After washing with a saturated aqueous NaHCO_3 twice to quench any remaining acid, the yellow solid was dissolved into toluene and subsequently recrystallized to form yellow crystals in 51% yield. ^1H NMR (400 MHz, deuterated chloroform) δ : 8.74 (d, 4 J = 2.35 Hz, 2H), 7.76 (dd, 3 J = 8.59, 4 J = 2.30 Hz, 2H), 7.49 (d, 3 J = 8.61 Hz, 2H).

Synthesis of 6-Bromo-*N,N*-Dimethylnaphthalen-2-Amine. (Compound 2)

6-Bromo-2-naphthol (Compound 1, 1.5 g, 6.7 mmol), a solution of dimethyl amine in methanol (15 mL, 33 mmol), and $\text{Na}_2\text{S}_2\text{O}_5$ (2.7 g, 13.6 mmol), were added to a reaction flask. Then, 5 mL of H_2O was added to the reaction flask in order to increase the solubility of $\text{Na}_2\text{S}_2\text{O}_5$, and the tube was then sealed. The reaction was slowly heated to 140 °C. After 40 h, the crude mixture was obtained by filtering the inorganic solid; the organic solution was washed with brine and DI-water three times and extracted with ethyl acetate. The mixture was purified by column chromatography (Hexane: ethyl acetate = 9:1 v/v) to yield a solid with 60% yield. ^1H NMR (400 MHz, deuterated chloroform) δ 7.84–7.80 (m, 1H), 7.63–7.57 (m, 1H), 7.51 (dq, J = 8.8, 0.6 Hz, 1H), 7.41 (dd, J = 8.8, 2.0 Hz, 1H), 7.16 (dd, J = 9.1, 2.6 Hz, 1H), 6.86 (d, J = 2.6 Hz, 1H), 3.05 (s, 6H).

Synthesis of *N,N*-Dimethyl-6-((Trimethylsilyl)Ethyne)Naphthalen-2-Amine (Compound 3)

$\text{Pd}(\text{PPh}_3)_2\text{Cl}_2$ (0.05 mmol), CuI (0.05 mmol), and 6-bromo-*N,N*-dimethylnaphthalen-2-amine (125 mg, 0.5 mmol) were added to a round bottle flask under a nitrogen blanket. Subsequently, freshly distilled diethyl amine (3 mL) with (trimethylsilyl) acetylene (0.14 mL, 1 mmol) were added to the flask. The reaction was slowly heated to 50 °C in the dark. After 24 h, the reaction mixture was diluted with ethyl acetate before being washed with brine and DI water three times. After the organic fraction was dried by Na_2SO_4 , the mixture was pushed through a silica gel flash column without further purification.

Synthesis of 4'-Bromo-*N,N*-Dimethyl-[1,1'-Biphenyl]-4-Amine (Compound 5)

4-(Dimethyl amino) phenylboronic acid pinacol ester (Compound 4, 494 mg, 2 mmol) and 1-bromo-4-iodobenzene (676 mg, 2.4 mmol) were added to a 20 mL sealed tube. Then, 0.1 equivalents of Pd (PPh_3)₄ (0.2 mmol) and Na_2CO_3 (6 mmol) were mixed and poured into the tube; 15 mL of THF and 2 mL of water were then injected to the tube. The tube was sealed and slowly heated to 80 °C overnight under a nitrogen atmosphere. The dark mixture that formed was washed with brine and then deionized (DI) water three times and extracted with ethyl acetate. After drying over Na_2SO_4 , the crude mixture was purified by silica gel column chromatography (hexane: ethyl acetate = 10:1 v/v) to give a solid with 40% yield. ^1H NMR (400 MHz, deuterated chloroform) δ 7.52–7.48 (m, 2H), 7.48–7.43 (m, 2H), 7.44–7.38 (m, 2H), 6.79 (d, J = 8.3 Hz, 2H), 2.99 (s, 6H).

Synthesis of *N,N*-Dimethyl-4'-((Trimethylsilyl)-Ethyne)-[1,1'-Biphenyl]-4-Amine (Compound 6)

$\text{Pd}(\text{PPh}_3)_2\text{Cl}_2$ (0.05 mmol), CuI (0.05 mmol), and 4'-bromo-*N,N*-dimethyl-[1,1'-biphenyl]-4-amine (Compound 5, 130 mg, 0.5 mmol) were added in a round bottom flask under a nitrogen blanket. Subsequently, freshly distilled diethyl amine (3 mL) and (trimethylsilyl) acetylene (0.14 mL, 1 mmol) were added to the flask. The reaction was slowly heated to 50 °C in the dark. After 24 h, the reaction mixture was diluted with ethyl acetate before being washed with brine and DI water three times. After the reaction, the organic fraction was dried with Na_2SO_4 , and the mixture was pushed through a silica gel flash column without further purification.

Synthesis of 2,7-Bis[[4-(Dimethylamino)Phenyl Ethynyl]-9H-Thioxanthene-9-One]

4-Ethyneyl-*N,N*-dimethylaniline (Compound 8, 362 mg, 2.5 mmol), $\text{Pd}(\text{PPh}_3)_2\text{Cl}_2$ (42 mg, 0.06 mmol), CuI (19 mg, 0.1 mmol), and DBTX (115 mg, 0.32 mmol) were added in a round bottle flask under nitrogen protection. Then freshly distilled diethyl amine (4 mL) was injected. The reaction was stirred for 30 h at 53 °C in the dark. The reaction mixture was diluted with ethyl acetate before being washed with brine and DI water three times. Afterwards, the organic layer was dried using Na_2SO_4 , the mixture was purified by column chromatography (Hexane:ethyl acetate = 6:1 v/v) to give a solid with 10% yield. It was mixed with

PETA immediately for use during nanoprinting because of its fast decomposition in air or exposure to light. ^1H NMR (400 MHz, deuterated chloroform) δ 7.89 (d, $J = 8.9$ Hz, 2H), 7.70 (d, $J = 8.0$ Hz, 2H), 7.49–7.41 (m, 4H), 7.39 (d, $J = 8.9$ Hz, 2H), 6.70–6.64 (m, 4H), 3.00 (s, 12H).

Synthesis of 2-Bromo-7-[(4-(Dimethylamino) Phenyl) Ethynyl]-9H-Thioxanthen-9-One

4-Ethynyl-*N,N*-dimethylaniline (Compound 8, 50 mg, 0.32 mmol), Pd(PPh₃)₂Cl₂ (14 mg, 0.02 mmol), CuI (10 mg, 0.05 mmol), and DBTX (115 mg, 0.32 mmol) were added to a round bottom flask under nitrogen protection. Freshly distilled diethyl amine (2 mL) was injected and the reaction was stirred for 24 h at 50 °C in the dark. The reaction mixture was diluted with ethyl acetate before being washed with brine and DI water three times. After the organic layer was dried with Na₂SO₄, the mixture was purified by column chromatography (hexane:ethyl acetate = 20:1 v/v) to produce a solid with 11% yield. ^1H NMR (400 MHz, deuterated chloroform) δ 8.74 (ddd, $J = 19.3, 2.1, 0.5$ Hz, 2H), 7.72 (ddd, $J = 8.4, 2.1, 1.5$ Hz, 2H), 7.56–7.47 (m, 2H), 7.47–7.41 (m, 2H), 6.68 (d, $J = 9.0$ Hz, 2H), 3.01 (s, 6H).

Synthesis of 2-Bromo-7-[(6-(Dimethylamino) Naphthalen-2-Yl)Ethynyl]-9H-Thioxanthen-9-One

N,N-dimethyl-6-((trimethylsilyl)-ethynyl)naphthalen-2-amine (Compound 3, 200 mg, 0.75 mmol), Pd(PPh₃)₂Cl₂ (28 mg, 0.04 mmol), CuI (19 mg, 0.1 mmol), and DBTX (115 mg, 0.32 mmol) were added in a round bottom flask under nitrogen protection. Freshly distilled diethyl amine (2 mL) was injected and the reaction was stirred for 30 h at 53 °C in the dark. The reaction mixture was diluted with ethyl acetate before being washed with brine and DI water three times. After the organic layer was dried with Na₂SO₄, the mixture was purified by column chromatography (hexane:ethyl acetate = 20:1 v/v) to give a solid with 8% yield. It was mixed with PETA immediately for use during nanoprinting because of its fast decomposition in air or exposure to light. ^1H NMR (400 MHz, deuterated chloroform) δ 8.77 (d, $J = 2.2$ Hz, 1H), 7.96–7.89 (m, 1H), 7.80–7.66 (m, 3H), 7.64–7.57 (m, 2H), 7.53–7.45 (m, 2H), 7.41–7.34 (m, 1H), 7.17 (ddd, $J = 9.1, 4.8, 2.6$ Hz, 1H), 6.88 (d, $J = 2.5$ Hz, 1H), 3.08 (s, 6H).

Computational Calculations Procedure

The theoretical ultraviolet-visible (UV-Vis) absorption spectra of the relevant molecules were calculated using Gaussian 09.¹⁹ The optimized ground-state geometries of all of the molecules were computed using DFT with the Becke 3-parameter hybrid functional with Lee–Yang–Parr correlation (B3LYP) and the 6-31G(d) basis set, as implemented in Gaussian 09. The optimized structures were verified by computing the infrared (IR) absorption spectra of the structure and verifying that no imaginary frequencies were present. After computing the optimized structures, the first 40 excited states of each molecule were computed using time-dependent DFT (TD-DFT) as implemented in Gaussian 09 at the same level of theory.

To generate the theoretical spectra, each excited state transition was used to generate a Gaussian function according to eq 2.²⁰

$$\varepsilon_i(\lambda) = a \times 10^8 \frac{f_i}{\sigma} \exp \left[- \left(\frac{(1/\lambda - 1/\lambda_i)}{\sigma} \right)^2 \right] \quad (2)$$

Here, a is a constant equal to 1.3062974, ε_i is the molar absorptivity of the molecule due to transition i at the given wavelength λ in units of L mol⁻¹ cm⁻¹, f_i is the oscillator strength of the transition, λ_i is the wavelength of the transition, and σ is standard deviation (representing the width of the Gaussian function). Because the available range for the standard deviation is from 0.2 eV to 0.8 eV, a default value of 3.226×10^{-4} nm⁻¹ (equal to 0.4 eV) was used in this calculation, as has been used previously.¹⁷ Summing the Gaussian functions for each transition provides the theoretical UV-Vis spectrum of the molecule. The complete tabular data for the S_n and T_n energy levels for the new photoinitiator of interest, BDAPT, are shown in the Supporting Information Tables S1 and S2, respectively.

DLW Photopolymerization

The excitation source consisted of a Ti:Sapphire oscillator (Coherent Mira-10) at 800 nm center wavelength and 80 MHz repetition rate. A continuous wave 638 nm diode laser was used as the inhibition beam, introduced via a dichroic beam splitter. Both beams were focused through a 100 \times objective lens (Nikon, N.A. = 1.49) to the sample located on a 100 μm \times 100 μm \times 200 μm travel piezostage (Mad City Labs), which is computer-controlled for translation in space. Fast mechanical shutters (Uniblitz) were used to control each beam independently. Attenuation of the laser power was achieved by variable neutral density filters. For each laser, a telescoping lens pair was used to expand the beam diameters before reaching the objective lens. The samples consisted of blends of monomer and photoinitiators sandwiched between a microscope slide and glass coverslip (thickness \sim 170 μm) with a single layer of Scotch tape providing a gap of \sim 40 μm . The concentration (by weight) of single photoinitiator in PETA monomer for each sample was 0.25% for BDAPT, 0.5% for both DANT and DAPT, and 1.5% for ITX. Coarse positioning of the sample was performed by a manual, micrometer-driven stage. The stages and objective lenses were mounted on an inverted microscope. All of the writing was performed at scan speed of 100 μm s⁻¹. Laser powers were measured at the back of the objective lens through a 6 mm diameter aperture. The heights of printed polymer lines were measured using an atomic force microscope (AIST NT) with a silicon tip in tapping mode. After these height measurements were made, the structures were sputter-coated with an Au/Pd mixture, and the samples were imaged using a scanning electron microscope (Hitachi S-4800) with 30 kV accelerating voltage.

Z-Scan Measurements

The nonlinear two-photon absorption cross sections were determined using an open-aperture Z-scan.²¹ All Z-scan measurements were performed using 50 fs pulses from a regeneratively amplified laser (KMLabs Wyvern-1000) with a center wavelength of 788 nm and full-width, half-maximum

(FWHM) bandwidth of 28 nm. The beam was first spatially filtered before being focused to a beam waist of $\sim 16 \mu\text{m}$. Solutions of photoinitiators in THF were evaluated with a 1 mm path length cuvette holding the solution. During the measurement, the sample was translated along the optical (z -) axis by a motorized stage. All of the transmitted signal was collected with a photodetector while a second photodetector measured the beam before the sample to remove any laser instability issues in the final reported data.

Excited State Lifetime Measurements

Excited state lifetimes of the photoinitiators were determined by transient absorption measurements using a collinear pump-probe scheme similar to a previous work.²² Here, the 800 nm pump beam was frequency doubled to 400 nm and the probe beam was set to 633 nm using an optical parametric amplifier (Quantronix TOPAS-C). The concentrations of ITX and BDAPT in THF were $8.2 \times 10^{-2} \text{ M}$ and $1.3 \times 10^{-3} \text{ M}$, respectively. The pump laser fluence was $\sim 1.4 \times 10^{-2} \text{ J cm}^{-2}$ for BDAPT and $\sim 1.2 \times 10^{-3} \text{ J cm}^{-2}$ for ITX. The probe laser fluence was $\sim 3.9 \times 10^{-4} \text{ J cm}^{-2}$ for BDAPT and $\sim 4.8 \times 10^{-4} \text{ J cm}^{-2}$ for ITX.

RESULTS AND DISCUSSION

As a commercially available photoinitiator, ITX has served as a model molecule that reveals the mechanism of energy transfer in two-photon DLW polymerizations, and the general picture of its operating mechanism in photopolymerizations is as follows. First, an electron in the ground state (S_0) of ITX is promoted to the first excited state (S_1) through a two-photon optical transition using an 800 nm wavelength laser.²³ Then, the excited state

undergoes intersystem crossing to generate the triplet state (T_1), which initiates the polymerization when ITX is blended with the monomeric species. As revealed by previous pump-probe spectroscopy experiments,^{12,23} the ITX molecule can undergo depletion of the excited state through both: (a) stimulated-emission depletion (STED) and (b) nonradiative decay by excitation of long-lived species in order to inhibit the polymerization. The latter of these two dominates in depletion DLW polymerization when ITX is the photoinitiator.^{12,23}

Due to the well-understood excited state dynamics of ITX, it is useful as a starting material for the development of high-performance polymerization photoinitiators. As such, the design of our photoinitiators is based on a previous work of the Gryko group.²⁴ Moreover, in order to guide the synthetic design, computational calculations were utilized to predict the absorption spectra of a set of potential photoinitiator molecules,¹⁹ and the experimentally synthesized materials were those that showed the most promise from these simulations. For example, relative to ITX, the peak absorption wavelength is red shifted for the BDAPT; 2-bromo-7-((6-(dimethylamino)naphthalen-2-yl)ethynyl)-9H-thioxanthen-9-one (DANT) and 2,7-bis((6-(dimethylamino)naphthalen-2-yl)ethynyl)-9H-thioxanthen-9-one (BDANT); 2-bromo-7-((4'-(dimethylamino)-[1,1'-biphenyl]-4-yl)ethynyl)-9H-thioxanthen-9-one (DEPT) and 2,7-bis((4'-(dimethylamino)-[1,1'-biphenyl]-4-yl)ethynyl)-9H-thioxanthen-9-one (BDEPT) compounds (Fig. 1).

This agrees with the concept that the extension of the π -system in photoinitiators can cause a redshift in the peak absorption of these ITX-based molecules. Moreover, there was a predicted redshift between the mono-substituted and the di-substituted derivatives as well. For example, in the predicted

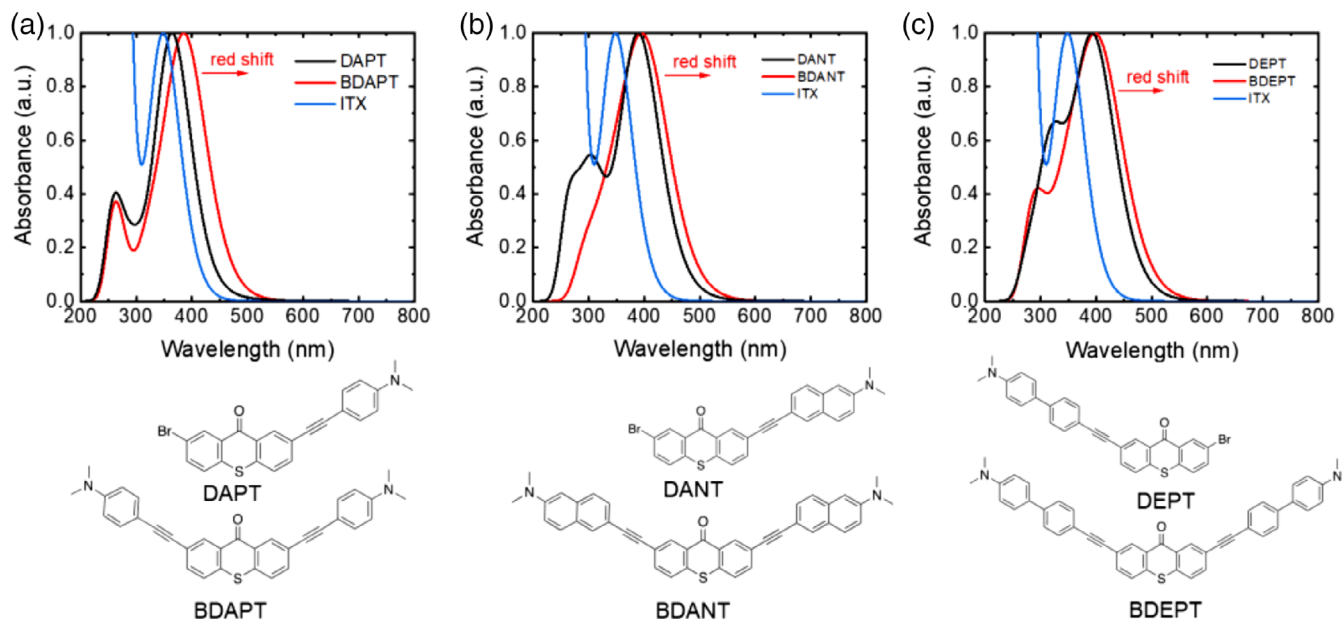


FIGURE 1 Predicted UV-Vis absorption plots for: (a) ITX, DAPT, and BDAPT; (b) ITX, DANT and BDANT; and (c) ITX, DEPT, and BDEPT. These predictions were made using TD-DFT with a B3LYP/6-31G(d) level of theory. The structures of the simulated photoinitiating molecules (aside from ITX) are shown directly below their calculated absorption spectra. [Color figure can be viewed at wileyonlinelibrary.com]

TABLE 1 Absorption Coefficients and Fluorescence Quantum Yields of the Photoinitiators

Photoinitiator	Solvent	Peak absorption wavelength (nm) ^a	Theoretical peak absorption wavelength (nm)	ϵ^b ($10^4 \text{ mol}^{-1} \text{ Lcm}^{-1}$)	ϵ^c ($10^4 \text{ mol}^{-1} \text{ Lcm}^{-1}$)	Φ_{fl} (%) ^e
ITX	Toluene	385	348	0.71	0.57	
	PETA	387		0.23	0.21	1.6
BDAPT	Toluene	408	390	0.91	0.83	
	PETA	414		2.0	1.8	8.1
DAPT	Toluene	353	365	5.1	1.2	
	PETA	– ^d		– ^d	– ^d	– ^d
DANT	Toluene	380	389	0.88	0.71	
	PETA	390		1.6	1.4	4.4
DBTX	Toluene	395		0.46	0.42	
	PETA	– ^d		– ^d	– ^d	– ^d

^a The peak wavelength is the maximum absorption near a wavelength of 400 nm if there are multiple peaks in the spectra.

^b The molar absorption coefficient of the species at the wavelength demonstrating the maximum absorption.

^c The molar absorption coefficient at the 390 nm wavelength.

^d Insufficient signal or difficult to dissolve in the PETA monomer.

^e Fluorescence quantum yield when the excitation wavelength was set to 390 nm.

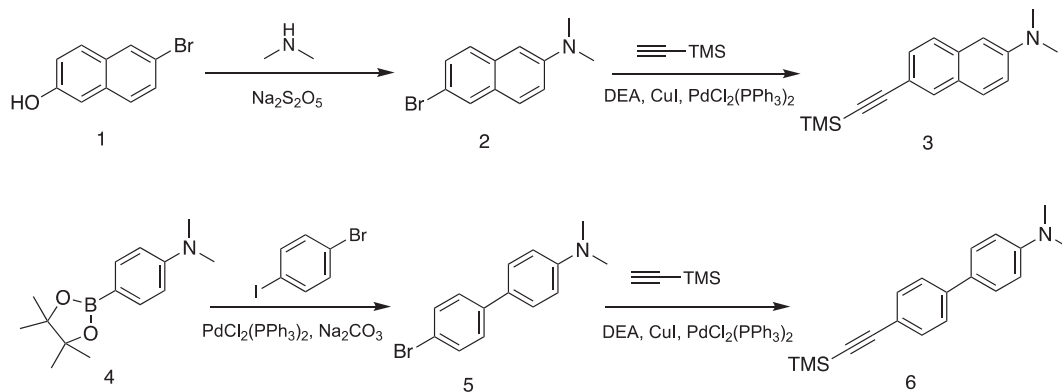
UV-Vis absorption data, the maximum absorption wavelength of BDAPT was redshifted about 25 nm relative to DAPT. This redshifted trend also was observed in the DANT- and DEPT-based systems due to the extension of the π -system.

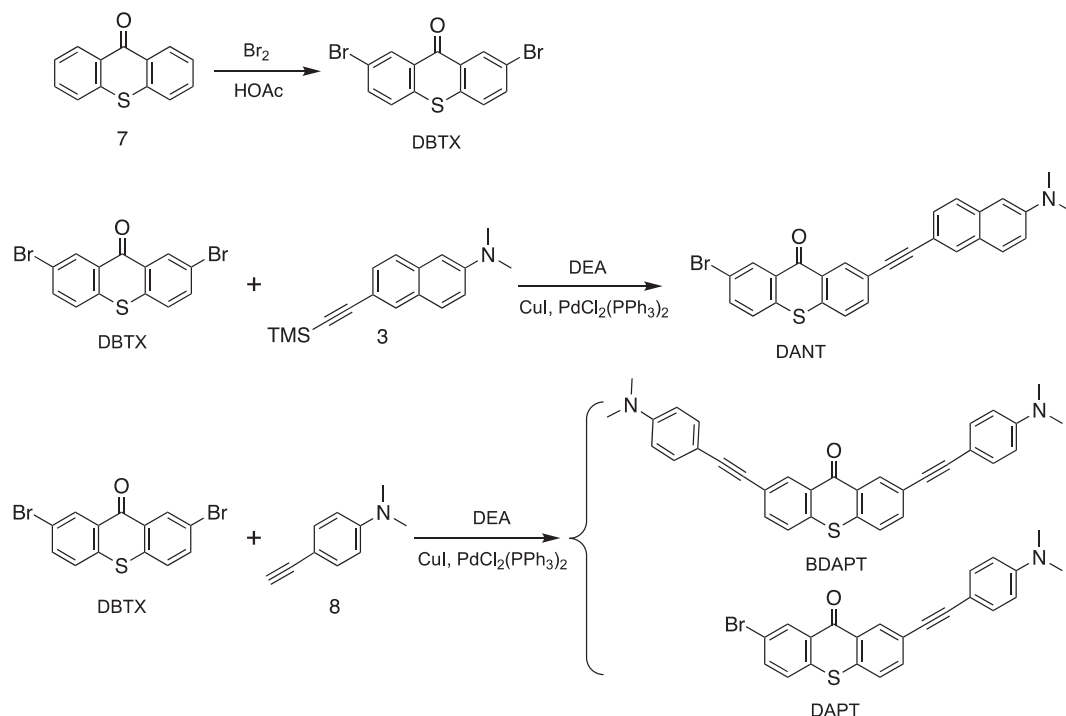
All the molecules have a relatively high predicted molar absorptivity coefficient at 400 nm (Table 1), which demonstrated their potential feasibility as efficient photoinitiators. Based upon these DFT results, the most promising compounds (i.e., DAPT, BDAPT, and DANT) were synthesized as these molecules exhibited strong absorption and were predicted to have maximum absorption wavelengths around 400 nm. Specifically, we designed a series of compounds based on an ITX core with different substituent groups. After our initial design, a straightforward series of high-throughput experiments (*vide infra*) were performed in order to down-select the most promising photoinitiating candidates. In this way, design and selection rules can be had for these types of photoinitiating systems.

In this particular effort, alkyne groups were introduced as linkers between the backbone and the branches for two major

reasons. First, this functionality increases the distance between the backbone and substituent branches to avoid steric hindrance effects, which may interrupt the conjugated system due to the possibility of rotation. Second, this functionality maintains aromaticity across the molecular system. Thus, functional groups were attached through the triple bond bridge. Specifically, phenyl, diphenyl, and naphthyl groups were synthesized and bonded through the alkyne group in a systematic way (Scheme 1). That is after a base-promoted aromatic substitution with dimethyl amine,²⁵ the naphthyl substituted group (Compound 3) was generated by a Sonogashira coupling reaction.²⁶ Similarly, the diphenyl-substituted group (Compound 6) was generated by a Pd-catalyst Suzuki coupling²⁷ followed by a Sonogashira coupling reaction.²⁸ Finally, the 4-ethynyl-*N,N*-dimethylaniline (Compound 8) was commercially available, and it was purchased directly from Sigma-Aldrich.

The synthetic pathway shown in Scheme 2 was then utilized to create the advanced photoinitiators, and these molecules were characterized by ¹H NMR spectroscopy and mass spectroscopy

**SCHEME 1** Synthetic pathway of the substituents of the photoinitiators.



SCHEME 2 Synthetic pathway for the advanced photoinitiators.

(Supporting Information Figs. S1–S3).^{26,28} Dibromothioxanthone-9-one (DBTX) can be synthesized through a bromination reaction.^{29–31} BDAPT and DAPT can be successfully formed by traditional Sonogashira coupling reactions using a single step.^{26,28,32} The major product of these reactions (i.e., either the di-substituted BDAPT or mono-substituted DAPT) can be controlled by changing the ratio of two different starting materials. DANT can also be generated through the same Sonogashira coupling in similar conditions; however, due to the instability of those species, the yield of DAPT, BDAPT, and DANT were low (11%, 10%, and 8%, respectively), and BDEPT, DEPT, and BDANT were not isolated in a manner that allowed for their evaluation as photoinitiating species.^{33,34}

After the successful syntheses according to Schemes 1 and 2, the frontier molecular orbitals were calculated and are shown in Figure 2. The thioxanthone core can be thought of as an acceptor and the (*N,N*-dimethylamino)phenyl moieties as the donors. The first two singlet excited states for BDAPT are transitions from the HOMO to the LUMO and from the HOMO–1 to the LUMO, respectively. These correspond to the intramolecular charge transfer states, as evidenced by the shift in the wave function density from the entire molecule to the thioxanthone center. The third calculated singlet excited state, which corresponds to the primary excitation at 400 nm, is a transition from the HOMO to the LUMO+1. This, by contrast, results in minimal change in the charge density on the molecule. Thus, the transition from S_1 to the lower optically inactive singlet states could proceed by a charge transfer mechanism.

The absorption and emission properties of the materials were characterized in order to compare their experimental

properties to the predicted properties and to evaluate their potential utility in the DLW photopolymerization process. In particular, synthesizing molecules with large molar absorptivity values at half the wavelength used in the DLW process (i.e., 400 nm) is of prime interest. Moreover, these same molecules should demonstrate relatively strong emission at the common depletion laser wavelength of 532 nm in their fluorescence spectra for quenching of the polymerization via the STED process. The normalized experimental UV–Vis absorption data are shown in Figure 3(a). DBTX was included in the result as a comparison in order to provide a baseline material that did not include any conjugated branches, and the experimental absorption spectrum of DBTX is redshifted relative to ITX. BDAPT and DANT had two broad peaks^{35,36} with relatively high absorbance at 400 nm, which can be attributed to the $\pi \rightarrow \pi^*$ transition at higher wavelength and $n \rightarrow \sigma^*$ jumping at lower wavelength due to the electron lone pair on the hetero atom.^{37,38} DAPT was also redshifted (Supporting Information Fig. S4), likely because of the charge transfer state generated by the asymmetric structure of DAPT.³⁹ As a result, all the new photoinitiators were redshifted as designed and had a relatively high absorption at 400 nm in UV–Vis spectrum (Supporting Information Fig. S4), such that the excitation processes occurred readily.

For light-induced inhibition of the DLW photopolymerization, ITX has been shown to predominantly follow a triplet–triplet absorption depletion pathway for the initiating species. However, for ITX derivatives such as these, there are other potential depletion pathways that may be non-negligible, or even dominating, for inhibiting the polymerization process.⁴⁰ In order to determine the possible contribution of another

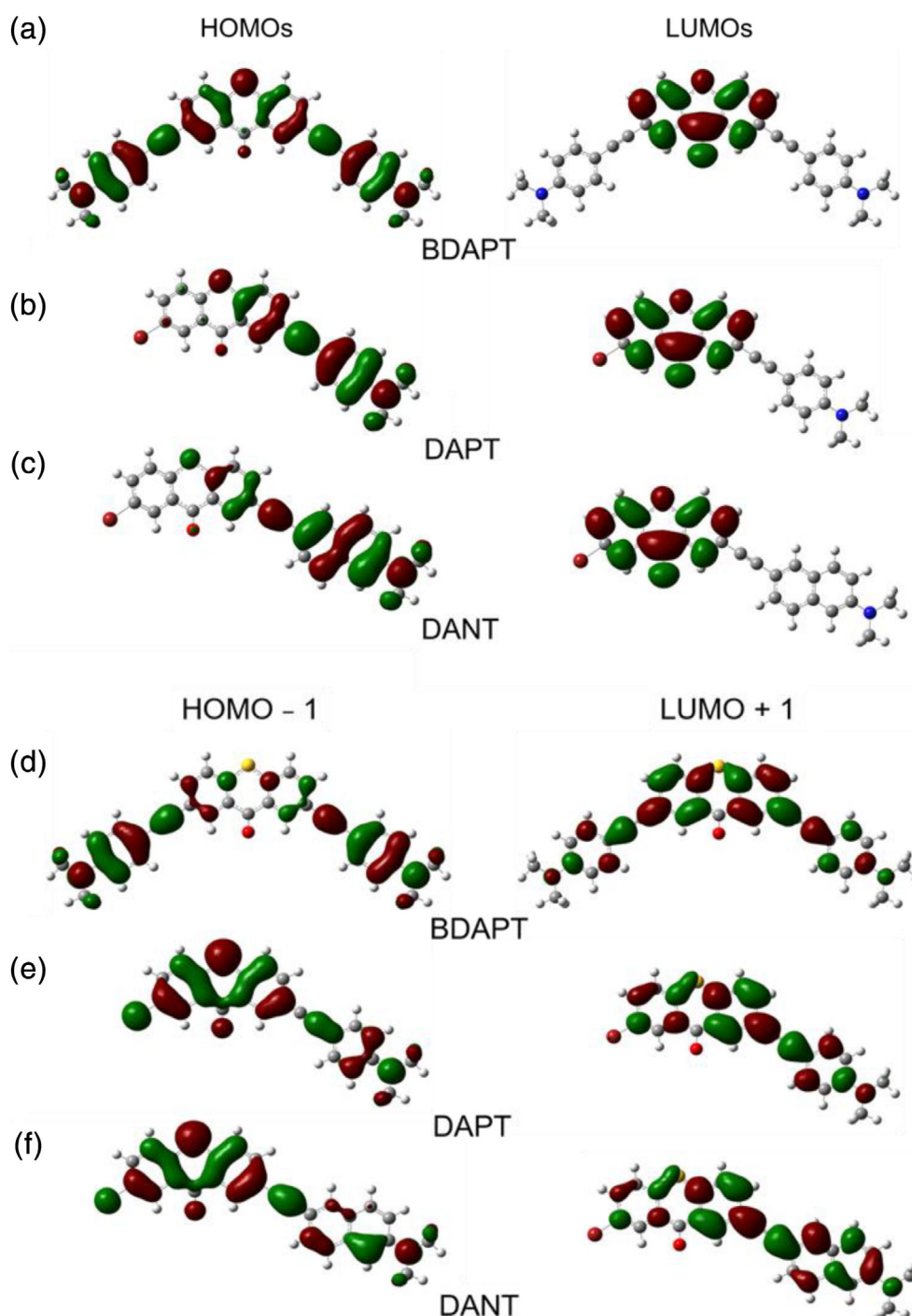


FIGURE 2 Molecular orbital diagrams calculated at an isovalue of 0.02. These plots are of the (a) HOMO, LUMO of BDAPT; (b) HOMO and LUMO of DAPT; (c) HOMO and LUMO of DANT; (d) HOMO-1 and LUMO+1 of BDAPT; (e) HOMO-1 and LUMO+1 of DAPT; and (f) HOMO-1 and LUMO+1 of DANT. They are used to illustrate the charge transfer states in those molecules. It can be seen that the HOMO, HOMO-1, and LUMO+1 wave functions are either spread over the entire molecule or localized to the *(N,N)*-dimethylamino phenyl moieties, while the LUMO wave functions are localized to the thioxanthone core. Therefore, electronic transitions from the highest two occupied orbitals to the LUMO should result in a transfer of charge from the branches to the core, while transitions to the LUMO+1 should not result in a charge transfer state formation. [Color figure can be viewed at wileyonlinelibrary.com]

popular depletion mechanism, stimulated emission depletion, to the polymerization inhibition process, the fluorescence of each molecule was established. The peak emission wavelength

trend of the different compounds is DBTX < ITX < DANT < DAPT < BDAPT [Fig. 3(b)]. Exposure of BDAPT at 532 nm may provide the greatest potential for STED because the peak

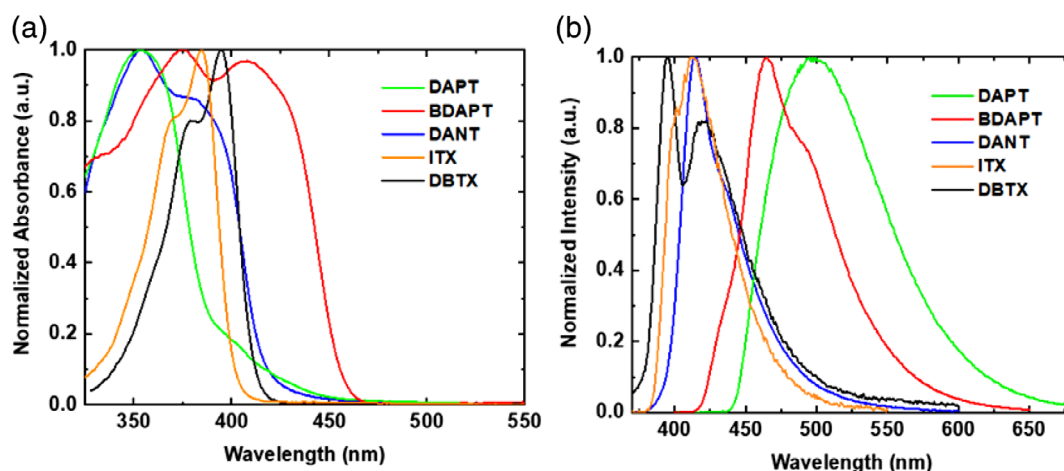


FIGURE 3 (a) The normalized UV-Vis absorbance spectra of photoinitiators in toluene. (b) The fluorescence spectra of the initiators in toluene obtained with excitation at 350 nm. [Color figure can be viewed at wileyonlinelibrary.com]

of fluorescence emission is approaching 532 nm. Excitation spectra were collected and compared to the absorption spectra. The spectra closely matched, indicating the observed emission is not due to an instrumentation artifact (Supporting Information Fig. S5). Thus, from both the UV-Vis and fluorescence spectra, BDAPT and DANT showed the potential to replace ITX as high-performing photoinitiators for DLW nanolithographic applications.

The coefficient of extinction and fluorescence quantum yield is listed in Table 1, and the raw data are presented in the Supporting Information Figure S6. All of the initiators, including ITX, had a relatively low fluorescence quantum yield in PETA, which indicated that the stimulated emission depletion process likely was not a dominant pathway and nonradiative decay from the excitation of long-lived species should be the major process for depletion. Therefore, any depletion effects exhibited in DLW with new initiators can be expected to follow a similar pathway as observed with ITX.

The extinction coefficient provides a clear representation of the ability of the photoinitiator to absorb light through a one-photon process; however, it was initially used here as an

indicator of the absorptive properties of the new initiators through a two-photon process. To directly measure the nonlinear absorption properties, an open-aperture Z-scan was performed for each of the photoinitiators.⁴¹ The measured two-photon absorption (TPA) cross sections, σ_2 , are presented in Table 2 along with the DLW polymerization writing thresholds for the initiators in PETA. The writing threshold power is the minimum laser power required to write a defined line structure that survives the development process.

For comparison purposes, the writing thresholds for each resist were calculated by dividing the photoinitiator concentration by the writing threshold power at $100 \mu\text{m s}^{-1}$. In order to account for unknowns in the Z-scan measurement, the ITX molecule with a known $\sigma_2^{13,22}$ was used as a reference to calibrate the measurement and obtain the presented values (see the Supporting Information). The trend of TPA cross sections is $\text{ITX} < \text{DBTX} < \text{DAPT} < \text{BDAPT} < \text{DANT}$. Although BDAPT and DANT trade spots in the TPA compared to their linear extinction coefficients determined through single-photon absorption, the simple extinction coefficient measurements provide reasonable indicators of the two-photon absorbing process (see Supporting Information Fig. S7 for the raw data for these measurements). Moreover, the new initiators, especially BDAPT and DANT, were much improved relative to the ITX TPA cross section and showed lower DLW polymerization thresholds; thus, they stood out as promising photoinitiating candidates.

Beyond improving the writing threshold for the DLW polymerization, it was necessary to investigate if the polymerization inhibition effect available in ITX was also present in the synthesized photoinitiators. To illustrate the depletion of the excited state, a 405 nm exciting laser was introduced orthogonally to a 633 nm laser beam and signal path [Fig. 4(a)]. In this configuration, the 633 nm laser was treated as the depletion laser. Assuming no saturation effects were occurring, if the addition of individual fluorescence signals for sample exposure by excitation (405 nm) and depletion (633 nm)

TABLE 2 Two-Photon Absorption Cross Section σ_2 and Writing Threshold of Photoinitiators

Photoinitiator	σ_2 (GM) ^a	Writing threshold (10^{18} molecules mW^{-1})
BDAPT	368 (± 45)	0.651
DANT	524 (± 61)	1.484
ITX	3 (± 0.4)	4.065
DAPT	122 (± 21)	– ^b
DBTX	22 (± 5)	– ^b

^a The values in parentheses indicate one standard deviation from the average measured value.

^b Difficulty dissolving this material uniformly in the monomer.

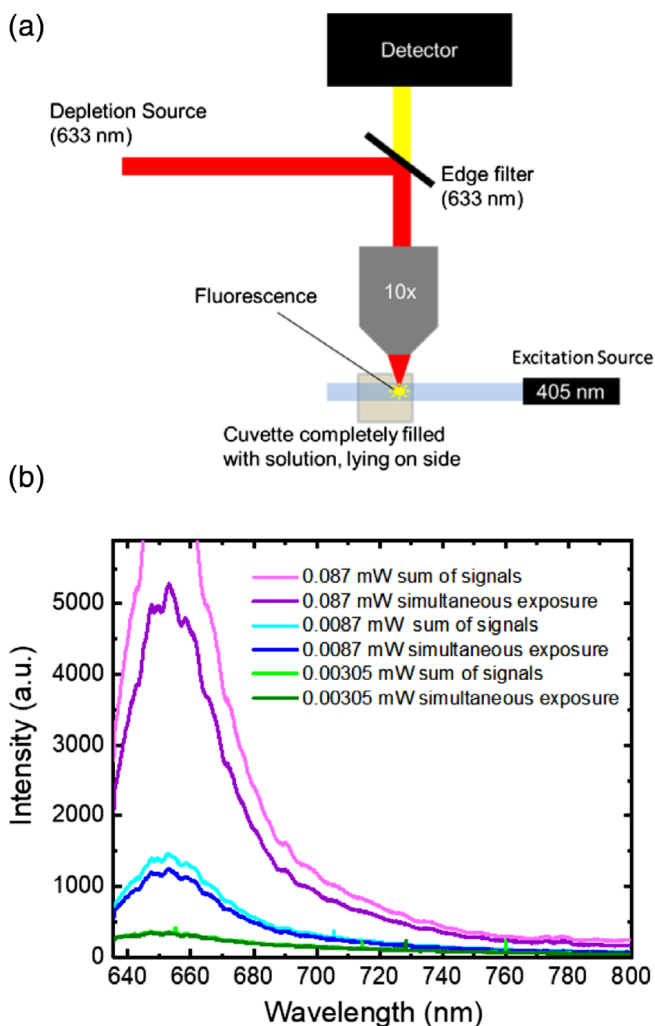


FIGURE 4 (a) A diagram of the experimental set-up for the two-laser spectroscopy system utilized to detect the depletion of select photoinitiators. (b) The fluorescence spectra with sum of individual excitation and depletion signals and the signal with both beams on simultaneously with 633 nm as depleting laser. The clear evidence of depletion was a good indicator of the ability to inhibit the photopolymerization process in actual DLW polymerization processes. As such, this photoinitiator was brought forward for complete DLW photopolymerization evaluation. [Color figure can be viewed at wileyonlinelibrary.com]

lasers was equal to the signal of when both the excitation and depletion sources were on, the photoinitiator responds to the each light independently. However, if the sum of individual signal was higher than the signal of both lasers when they were in the on state, depletion of the fluorescing state of the photoinitiator occurred. Alternatively, additional absorption was said to be detected if the sum of the individual signals was lower than that of the signals when both lasers were in the on state. For the BDAPT in THF solution shown in Figure 4(b), three different depletion laser powers were tested, and the 405 nm wavelength excitation power was held constant. For all three depletion intensities, the sum of individual signals was greater than the signal with both lasers on

indicating a depletion of the BDAPT excited state by the 633 nm laser.

This effect was not observed when 633 nm laser was replaced with 532 nm laser. Many factors contribute to a successful photoinitiator for the DLW photopolymerization process, making it difficult to accurately predict its exact performance during actual printing conditions. Specifically, the polymerization inhibition effect is not easily measured outside of a direct test inside a monomer matrix. Due to its performance in the aforementioned experiments, BDAPT was selected for its potential ability to perform in the DLW photopolymerization process. In particular, BDAPT showed promise with respect to the aforementioned two-laser system, due to its large TPA cross section, and due to its relatively large solubility in the PETA monomer compared to DANT. For this evaluation, a 638 nm laser was spatially overlapped with the DLW 800 nm beam and a Gaussian profile is used for both beams; care was taken to ensure that the focused 638 nm beam diameter was at least as large as the DLW spot. The depletion laser wavelength of 638 nm was chosen as a result of the above fluorescence depletion experiments. BDAPT at a loading of 0.25 wt % in PETA was used as the test photoresist. As shown in Figure 5, a group of parallel polymer lines were printed using the DLW polymerization process. During the writing of each line, the sample was exposed to the 638 nm laser for 10 μm of the line path without turning off the DLW beam. During that time of exposure to the inhibition beam, which correlated with 10 μm in space, the polymerization was fully inhibited. It is worth noting, however, that the conditions to observe this effect required careful control of the DLW beam power slightly below the writing threshold. This led to the poor quality of printed lines observed in the figure. Beyond that, the 638 nm laser power required for inhibiting the polymerization was large compared to using ITX as photoinitiator.

In order to elucidate the inhibition effects for BDAPT, ultra-fast transient absorption experiments were performed on BDAPT and ITX [Fig. 6(a)]. A wavelength of 400 nm was used as the pump in order to excite the S_1 state of the molecules, in a manner similar to other studies.²¹ This wavelength matched the induced transition of the two-photon absorption occurring during the DLW polymerization process with a 800 nm laser, and it allowed for more uniform pumping of the molecules to the excited state with a lower pump laser power. The probe wavelength was chosen to be 633 nm. Two lifetimes were fit for both ITX ($\tau_1 = 30.2$ ps, $\tau_2 = 4.2$ ns) and BDAPT ($\tau_1 = 6.9$ ps, $\tau_2 = 187$ ps). In the case of ITX, because the pump energy closely matches the S_1 energy level, the fast lifetime (τ_1) is attributed to the S_1^* states, and the longer lifetime is attributed to the S_1 state, which is consistent with a previous report.²¹ In other words, τ_1 represents how fast S_1 is filled while τ_2 is the rate at which S_1 is depopulated, where some of the population from the S_1 state was transferred to the longer-lived triplet state, which initiates polymerization. In this scenario, the probe beam is interacting with a $S_1 \rightarrow S_n$ transition.

In the case of BDAPT, a proposed probe interaction was with respect to both the $S_1 \rightarrow S_n$ and the $S_1^* \rightarrow S_n$ transitions. A sharp

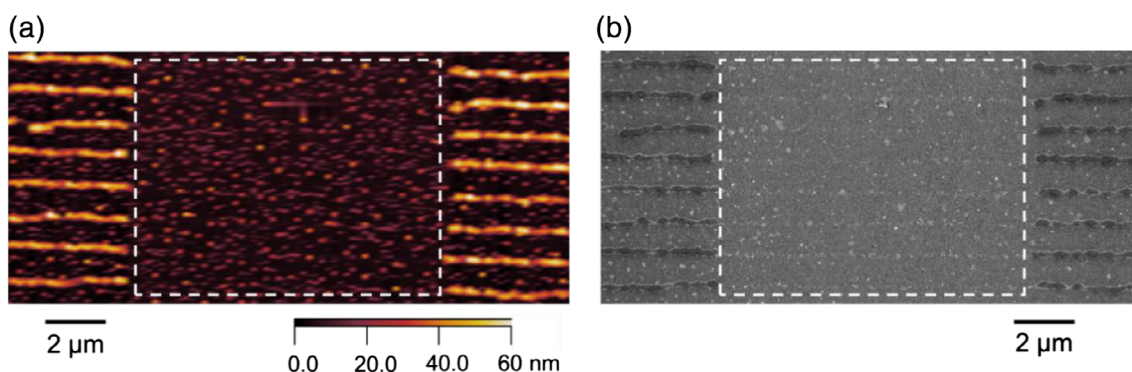


FIGURE 5 Selectively inhibited DLW photopolymerization using BDAPT (0.25 wt %) as a photoinitiator in the PETA monomer. Polymer lines were written at $100 \mu\text{m s}^{-1}$ with the 638 nm diode laser turned on for 10 μm , preventing polymerization in the region shown by the box highlighted by white dashed lines. (a) The AFM image of the printed polymer nanoscale lines. (b) The SEM image of the same polymer lines. [Color figure can be viewed at wileyonlinelibrary.com]

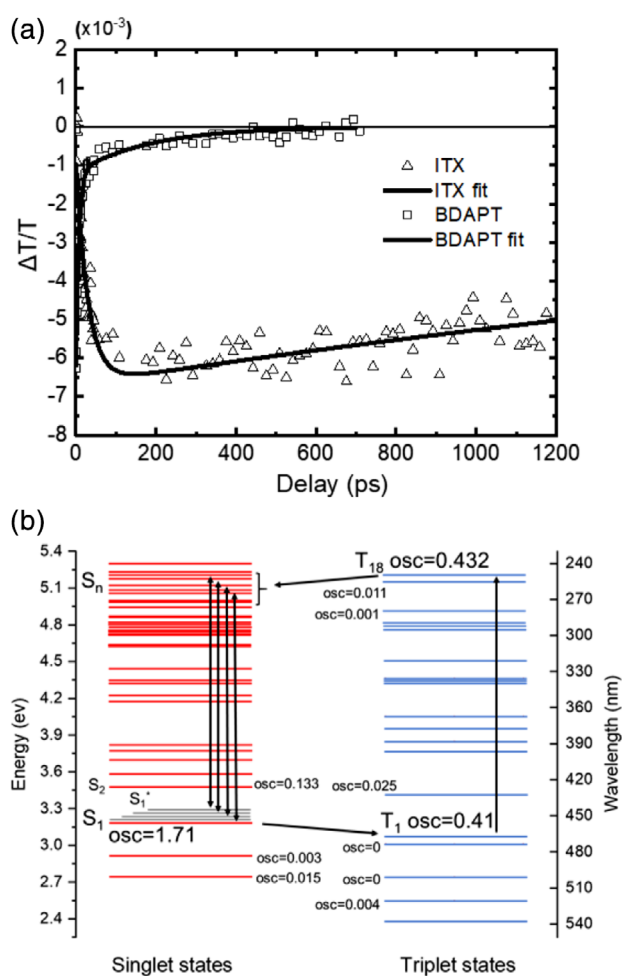


FIGURE 6 (a) Ultra-fast transient absorption measurement of ITX and BDAPT in THF. The pump and the probe wavelengths used were 400 nm and 633 nm, respectively. The solid lines represent fits to the data, which is shown as either open triangles (ITX) or open squares (BDAPT). (b) The DFT calculation of the singlet states and triplet states of BDAPT and the most likely pathway of depletion. S_1^* levels are not calculated and are sketched for visualization purposes only. [Color figure can be viewed at wileyonlinelibrary.com]

initial drop in the transmission curve occurred on a timescale comparable with the pulse duration, where S_1 and S_1^* were filled by the pump beam. The $S_1^* \rightarrow S_1$ intraband transition was then observed to have a lifetime of τ_1 , which was about four times shorter than for ITX. A final S_1 lifetime of τ_2 (187 ps) for BDAPT was found to be about 22 times shorter than τ_2 (4.2 ns) for ITX. As shown in the calculations of Figure 6(b), BDAPT was predicted to undergo a $T_1 \rightarrow T_n$ transition.¹² The calculated energy gap between T_1 and T_{18} was 581 nm, which is smaller than the depleting laser used during lithography because the energy gap in PETA solution is different from the energy gap with no solvent present.^{42,43} This led to the inhibition of the polymerization by depopulating the T_1 state before polymerization occurred, similar to the mechanism commonly associated with depletion in ITX-based systems.¹² It is crucial to notice that the lifetime of the S_1 state (187 ps) for BDAPT is much shorter than the lifetime of S_1 state (4.2 ns) for ITX. This large difference leads to a sizeable population of BDAPT entering the T_1 state in a short period of time. T_1 is the energy state leading to polymerization during nanoprinting, which is why BDAPT can initiate writing at a fivefold lower power than ITX.

To provide insights into the T_1 lifetimes, phosphorescence spectra at a temperature of 77 K were acquired. As shown in Figure 7, all the initiators possess clear phosphorescent emission, which indicates that the depletion of singlet-excited state via intersystem crossing to the triplet state exists in all of the systems evaluated here. The trend of the phosphorescent lifetimes is DBTX (10 ms) < ITX (120 ms) < DAPT (219 ms) < BDAPT (287 ms) < DANT (379 ms), which represents the sequence of how long the molecules would have their T_1 states populated. When comparing DBTX, DAPT, and BDAPT (Fig. 8), we establish that the addition of conjugated branches increases the phosphorescence lifetime, although the effect is decreased when the second branch is introduced.

By comparing DAPT and DANT, we see that the naphthalene substituent performs differently than phenyl substituent to increase the phosphorescence lifetime. This indicates that the structure design of branches has a significant impact on this

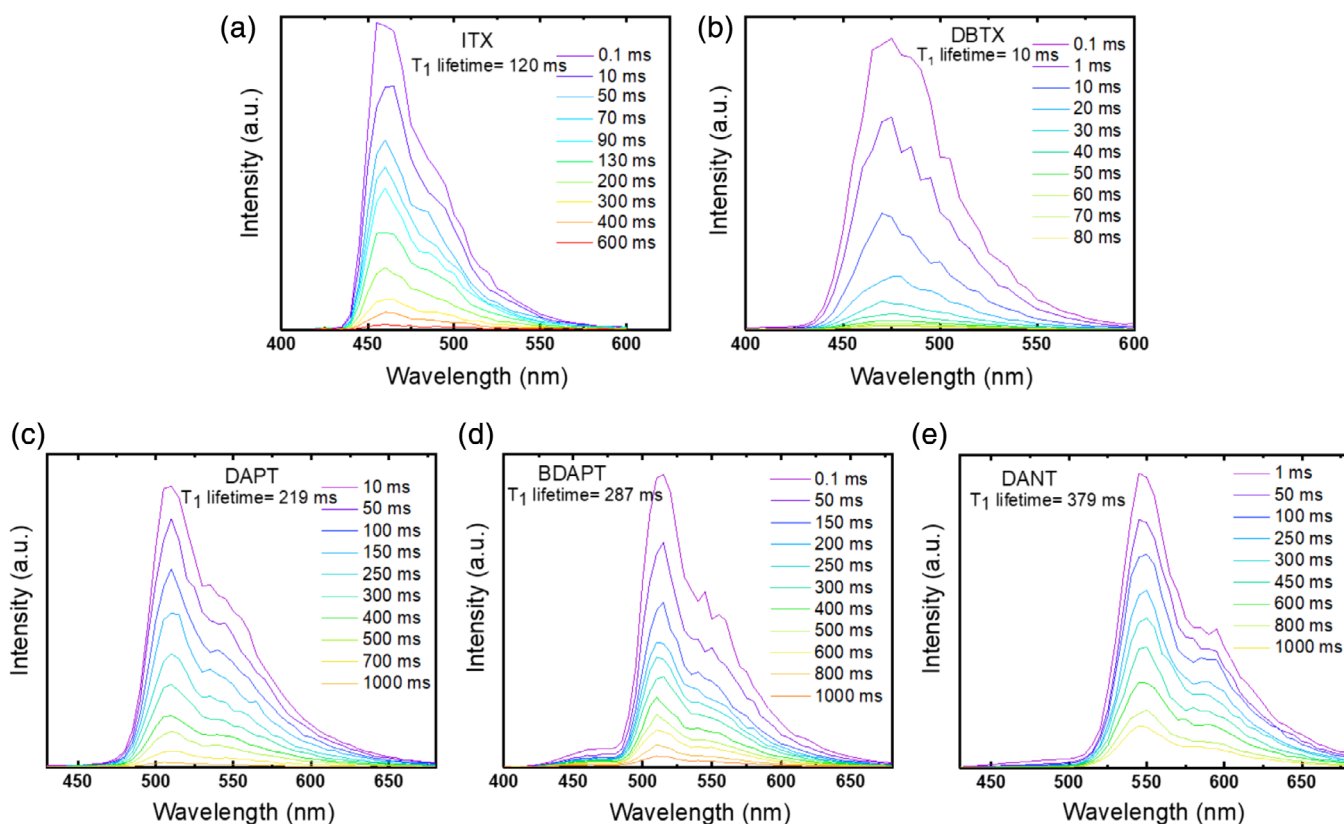


FIGURE 7 Phosphorescence spectra of the photoinitiators in toluene at $T = 77$ K after excitation at 350 nm. The spectra shown are: (a) ITX with a lifetime of 120 ms; (b) DBTX with a lifetime of 10 ms; (c) DAPT with a lifetime of 219 ms; (d) BDAPT with a lifetime of 287 ms; and (e) DANT with a lifetime of 379 ms. [Color figure can be viewed at wileyonlinelibrary.com]

photophysical property. Note that ITX has a moderate phosphorescence lifetime that is shorter than DAPT, BDAPT, and DANT. This informs us that the triplet lifetime is not the only significant determining factor for efficient depletion. ITX

seems to demonstrate an efficient $T_1 \rightarrow T_n$ transition allowing easy depletion of the printing. In the case of BDAPT, the $T_1 \rightarrow T_n$ transition was not efficient enough to fully depopulate the T_1 state, which explains why partial depletion was

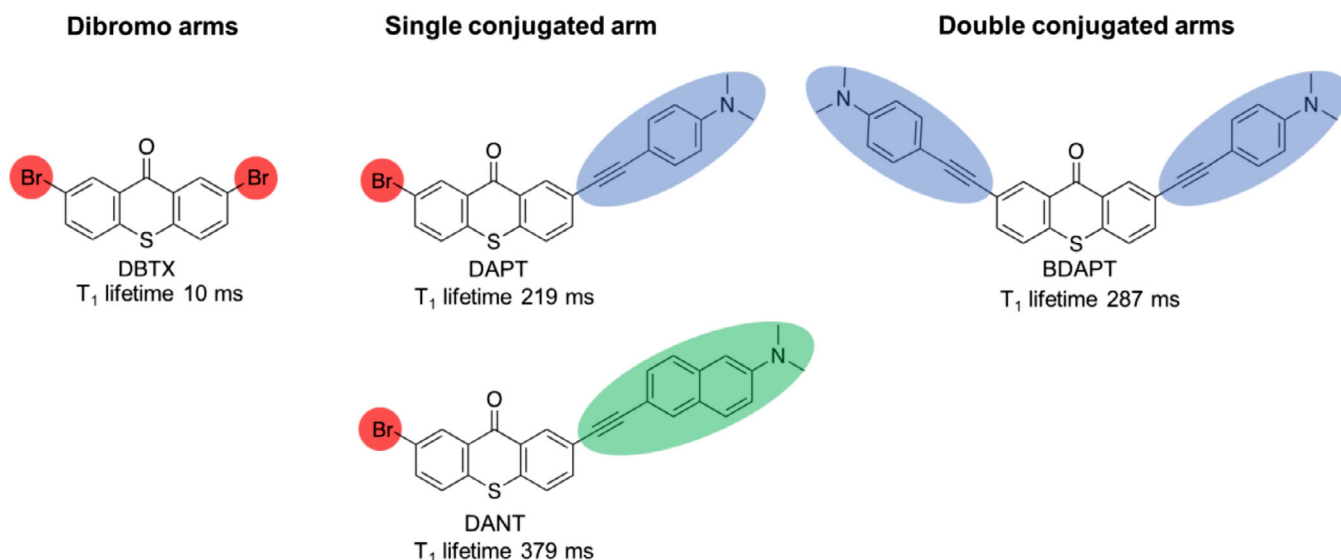


FIGURE 8 The influence of replacing the Br atom by either a single conjugated branch or two conjugated branches to the corresponding T_1 lifetime. These results indicate that both the exact chemistry and the degree of conjugation (for the same chemistry) can alter the lifetimes of the T_1 states for these ITX-based molecules. [Color figure can be viewed at wileyonlinelibrary.com]

observed in lithography with low depleting power, but full depletion was challenging to achieve (Supporting Information Figs. S8 and S9). To summarize, the moderate population of ITX on the T_1 state brings about moderate writing power and moderate depleting power, but the extreme population of BDAPT on the T_1 state leads to a lower writing power and a higher depleting power. Consequently, compared to ITX, our new initiator is much more efficient in initiating the DLW photopolymerization process but trades this advantage for a reduced polymerization inhibition capability. Therefore, this molecule could be of significant interest in applications requiring low laser power (i.e., high throughput, multiple-writing laser situations); however, additional effort could be placed in decreasing the inhibition threshold of the next-generation photoinitiators.

CONCLUSIONS

In this work, we developed and synthesized several new photo-initiating species based on a thiophene-9-one core and carried the most promising molecule forward as the photoinitiator for DLW photopolymerization. The extension of the π -system of our initiators led to a redshift of the visible light absorption toward the direction of the desired 400 nm peak (i.e., at half the wavelength of the pulsed writing laser). Moreover, this molecular feature increased the molar extinction coefficient of BDAPT relative to the ITX core. BDAPT demonstrated a fivefold decrease in threshold writing power compared to ITX for the photopolymerization of interest, which is key in minimizing energy requirements and for the potential to use these materials in high throughput photopolymerization writing. Beyond that, BDAPT had photopolymerization inhibition capabilities under DLW when an additional depletion laser was used. Ultrafast spectroscopic experiments, low-temperature phosphorescence spectroscopy and DFT calculations were used to explain the mechanism of both excitation and depletion of BDAPT. These data indicate that a short excited state lifetime leads to poor inhibition of photopolymerization due to a strongly populated triplet state with inefficient triplet-triplet absorption depletion pathway. Therefore, we have proposed a practical direction to modify and improve existing photoinitiators for two-photon DLW photopolymerization. In turn, this should allow for the ready modification of existing photoinitiators in the future 3D nanoprinting photopolymerization reactions, for not only ITX-based systems but for more exotic systems as well, by providing insights into the critical properties of a photoinitiator molecule that leads to a desired photopolymerization performance and how to tailor a photoinitiating molecule to achieve those properties.

ACKNOWLEDGMENTS

This work was supported by the National Science Foundation (NSF) through the Scalable Nanomanufacturing Program (Award Number: 1634832, Program Manager: Dr. Khershed Cooper), and we thank the NSF for their gracious support. We thank Mr. Duanchen Ding from the group of Professor Hilka I. Kenttämä at Purdue University for his assistance regarding

mass spectrometry data. We thank Dr. Xikang Zhao for helpful discussions.

REFERENCES AND NOTES

- 1 S. Maruo, O. Nakamura, S. Kawata, *Opt. Lett.* **1997**, *22*, 132.
- 2 S. Kawata, H.-B. Sun, T. Tanaka, K. Takada, *Nature* **2001**, *412*, 697.
- 3 M. Deubel, G. von Freymann, M. Wegener, S. Pereira, K. Busch, C. M. Soukoulis, *Nat. Mater.* **2004**, *3*, 444.
- 4 G. von Freymann, A. Ledermann, M. Thiel, I. Staude, S. Essig, K. Busch, M. Wegener, *Adv. Funct. Mater.* **2010**, *20*, 1038.
- 5 F. Klein, B. Richter, T. Striebel, C. M. Franz, G. v. Freymann, M. Wegener, M. Bastmeyer, *Adv. Mater.* **2011**, *23*, 1341.
- 6 V. Melissinaki, A. Gill, I. Ortega, M. Vamvakaki, A. Ranella, J. Haycock, C. Fotakis, M. Farsari, F. Claeysens, *Biofabrication* **2011**, *3*, 045005.
- 7 S. W. Hell, *Phys. Lett. A* **2004**, *326*, 140.
- 8 S. W. Hell, J. Wichmann, *Opt. Lett.* **1994**, *19*, 780.
- 9 J. Fischer, G. von Freymann, M. Wegener, *Adv. Mater.* **2010**, *22*, 3578.
- 10 J. Fischer, J. B. Mueller, A. S. Quick, J. Kaschke, C. Barner-Kowollik, M. Wegener, *Adv. Opt. Mater.* **2015**, *3*, 221.
- 11 L. Li, R. R. Gattass, E. Gershgoren, H. Hwang, J. T. Fourkas, *Science* **2009**, *324*, 910.
- 12 B. Harke, W. Dallari, G. Grancini, D. Fazzi, F. Brandi, A. Petrozza, A. Diaspro, *Adv. Mater.* **2013**, *25*, 904.
- 13 K. J. Schafer, J. M. Hales, M. Balu, K. D. Belfield, E. W. Van Stryland, D. J. Hagan, *J. Photochem. Photobiol. A Chem.* **2004**, *162*, 497.
- 14 W. Schnsbel, *Polymers and Light*; Wiley-VCH: Weinheim, **2007**, p. 305.
- 15 M. Malinauskas, A. Žukauskas, G. Bičkauskaitė, R. Gadonas, S. Juodkasis, *Opt. Express* **2010**, *18*, 10209.
- 16 B. H. Cumpston, S. P. Ananthavel, S. Barlow, D. L. Dyer, J. E. Ehrlich, L. L. Erskine, A. A. Heikal, S. M. Kuebler, I. Y. S. Lee, D. McCord-Maughon, J. Qin, H. Röckel, M. Rumi, X.-L. Wu, S. R. Marder, J. W. Perry, *Nature* **1999**, *398*, 51.
- 17 T. Serevičius, R. Komskis, P. Adomėnas, O. Adomėnienė, V. Jankauskas, A. Gruodis, K. Kazlauskas, S. Juršėnas, *Phys. Chem. Chem. Phys.* **2014**, *16*, 7089.
- 18 H. J. Yvon, *HORIBA*; Jobin Yvon Ltd.: Stanmore, Middlesex, UK, **2012**.
- 19 M. Frisch, G. Trucks, H. Schlegel, G. Scuseria, M. Robb, J. Cheeseman, G. Scalmani, V. Barone, G. Petersson, H. Nakatsuji, Gaussian Inc., Wallingford, CT **2016**.
- 20 UV Plots from the Results of Excited States Calculations, <http://gaussian.com/uvvisplot/> (accessed July 2018)
- 21 M. Sheik-Bahae, A. A. Said, T. Wei, D. J. Hagan, E. W. V. Stryland, *IEEE J. Quantum Electron.* **1990**, *26*, 760.
- 22 C. Chen, I. Vasudevan, Z. Du, X. Xu, L. Pan, *Appl. Phys. Lett.* **2018**, *112*, 253105.
- 23 T. J. A. Wolf, J. Fischer, M. Wegener, A.-N. Unterreiner, *Opt. Lett.* **2011**, *36*, 3188.
- 24 R. Nazir, E. Balčiūnas, D. Buczyńska, F. Bourquard, D. Kowalska, D. Gray, S. Maćkowski, M. Farsari, D. T. Gryko, *Macromolecules* **2015**, *48*, 2466.
- 25 A. S. Rao, D. Kim, T. Wang, K. H. Kim, S. Hwang, K. H. Ahn, *Org. Lett.* **2012**, *14*, 2598.
- 26 K. Sonogashira, *J. Organomet. Chem.* **2002**, *653*, 46.
- 27 J. Kulhánek, F. Bureš, M. Ludwig, *Beilstein J. Org. Chem.* **2009**, *5*, 11.

- 28** K. Sonogashira, Y. Tohda, N. Hagihara, *Tetrahedron Lett.* **1975**, *16*, 4467.
- 29** M. P. Coleman, M. K. Boyd, *J. Org. Chem.* **2002**, *67*, 7641.
- 30** S. Dadashi-Silab, H. Bildirir, R. Dawson, A. Thomas, Y. Yagci, *Macromolecules* **2014**, *47*, 4607.
- 31** L. Ding, Z. Zhang, X. Li, J. Su, *Chem. Commun.* **2013**, *49*, 7319.
- 32** W. Shi, Y. Luo, X. Luo, L. Chao, H. Zhang, J. Wang, A. Lei, *J. Am. Chem. Soc.* **2008**, *130*, 14713.
- 33** Y. Liu, N. Gu, P. Liu, J. Xie, X. Ma, Y. Liu, B. Dai, *Appl. Organomet. Chem.* **2015**, *29*, 736.
- 34** S. Xu, Z. Yun, Y. Feng, T. Tang, Z. Fang, T. Tang, *RSC Adv.* **2016**, *6*, 69822.
- 35** J. Yang, A. Dass, A.-M. M. Rawashdeh, C. Sotiriou-Leventis, M. J. Panzner, D. S. Tyson, J. D. Kinder, N. Leventis, *Chem. Mater.* **2004**, *16*, 3457.
- 36** K. D. Thériault, C. Radford, M. Parvez, B. Heyne, T. C. Sutherland, *Phys. Chem. Chem. Phys.* **2015**, *17*, 20903.
- 37** A. K. R. Junker, T. J. Sørensen, *Methods Appl. Fluores.* **2017**, *6*, 014002.
- 38** D. A. Skoog, F. J. Holler, S. R. Crouch, *Principles of Instrumental Analysis*; Cengage Learning: Boston, MA, **2017**.
- 39** B. Dereka, A. Rosspeintner, Z. Li, R. Liska, E. Vauthey, *J. Am. Chem. Soc.* **2016**, *138*, 4643.
- 40** T. A. Klar, S. Jakobs, M. Dyba, A. Egner, S. W. Hell, *Proc. Natl. Acad. Sci.* **2000**, *97*, 8206.
- 41** B. Gu, Y.-X. Fan, J. Wang, J. Chen, J. Ding, H.-T. Wang, B. Guo, *Phys. Rev. A* **2006**, *73*, 065803.
- 42** M. Glukhovtsev, *J. Chem. Inf. Comput. Sci.* **1997**, *37*, 1206.
- 43** E. Fabiano, F. D. Sala, R. Cingolani, M. Weimer, A. Görling, *Chem. A Eur. J.* **2005**, *109*, 3078.